*Journal of Alloys and Compounds, 185* (1992) 221–234
*JALCOM 196*



# $Ca_{8-x}Li_xAl_3$: defects and substitution in the $Fe_3Al$ structure type

Gordon J. Miller* and Reinhard Nesper**
*Max-Planck-Institut für Festkörperforschung, Heisenbergstrasse 1, 7000 Stuttgart 80 (Germany)*

(Received November 26, 1991)

## Abstract

$Ca_{8-x}Li_xAl_3$ was obtained in crystalline form during investigations of the Ca–Li–Al ternary phase diagram. The structure is isotypic to $Ca_8In_3$ (space group $P\bar{1}$; $a=947.0$ pm, $b=960.2$ pm, $c=964.6$ pm, $\alpha=99.17°$, $\beta=101.08°$, $\gamma=119.51°$), which is an ordered defect structure of the $Fe_3Al$ or the $Li_3Bi$ type. Vacancies occur exclusively at pseudotetrahedral sites and lithium substitutes for calcium in the pseudo-octahedral sites when compared with the cubic $Fe_3Al$ structure (space group $Fm\bar{3}m$) of a hypothetical "$Ca_3Al$". Madelung and extended Hückel calculations are utilized to discuss the observed defect and substitutional pattern.

## 1. Introduction

In the Ca–Al binary system, only two phases have been characterized: $CaAl_2$ (cubic $MgCu_2$–type) [1, 2] and $CaAl_4$ (tetragonal $BaAl_4$ type) [3]. No calcium-rich phases are yet known. With gallium and indium, Fornasini and Pani have reported two calcium-rich compounds: $Ca_{28}Ga_{11}$ [4] and $Ca_8In_3$ [5], the second of which is the so called "$Ca_3In$" phase in the Ca–In system. During efforts to examine the Ca–Li–Al ternary diagram, we discovered crystals which, after an X-ray structure determination, exhibit geometrical characteristics of the $Ca_8In_3$ structure, but are deficient in calcium. In this contribution we shall present the structure determination of $Ca_{8-x}Li_xAl_3$, a comparison with related compounds, and comments regarding the importance of lithium in this material.

## 2. Experimental details

The sample was prepared by melting ($T=1180$ K) a mixture of calcium (99.5 at.%, Fluka), lithium (99 at.%, Merck), and aluminium (99.9 at.%,

*Present address: Department of Chemistry, Iowa State University, Ames, IA 50011, USA.
**Present address: Laboratorium für Anorganische Chemie, ETH Zentrum, CH-8092 Zürich, Switzerland.

0925-8388/92/$5.00

Merck) in the ratio 4:1:1 in a molybdenum crucible, which was sealed in a niobium ampoule under an argon atmosphere. The reaction container was placed in an argon-filled quartz Schlenk tube. After 2 h the melt was slowly cooled to room temperature over a 2 day period. Attempts to prepare a pure binary $Ca_8Al_3$ phase failed under similar conditions.

A crystal suitable for data collection (checked with Buerger precession photographs) was mounted in an argon-filled capillary and measured on a single-crystal diffractometer. Solution of the structure proceeded with direct methods in space group $P\bar{1}$. Table 1 contains all crystal data and refinement parameters. Atomic coordinates and anisotropic temperature factors are listed in Table 2, and significant bond distances are given in Table 3.

TABLE 1

Crystallographic data for $Ca_{8-x}Li_xAl_3$ ($x=0.16$)

| | |
|---|---|
| Empirical formula | $Ca_{15.68}Li_{0.32}Al_6$ |
| Crystal size ($mm^3$) | $0.06\times0.03\times0.05$ |
| Crystal system | Triclinic |
| Space group | $P\bar{1}$ |
| $a$, $b$, $c$ (pm) | 947.0(2), 960.2(2), 964.6(2) |
| $\alpha$, $\beta$, $\gamma$ (deg) | 99.17(2), 101.08(2), 119.50(2) |
| Volume ($pm^3$) | $715.2(3)\times10^6$ |
| $Z$ | 1 |
| Formula weight (Da) | 790.4 |
| Density (calculated) ($Mg\ m^{-1}$) | 1.835 |
| Absorption coefficient ($mm^{-1}$) | 3.021 |
| $F(000)$ | 391.63 |
| Diffractometer; radiation | Siemens R3m/V; Mo K$\alpha$ ($\lambda=0.71073$ Å) |
| Temperature (K) | 298 |
| Monochromator | Highly oriented graphite crystal |
| $2\theta$ range (deg) | 4.0–55.0 |
| Scan type; speed; range | $\omega$; variable; 0.50–19.50° $min^{-1}$ in $\omega$; 2.00° |
| Standard reflections | 2 measured every 98 reflections |
| Index ranges | $-12\leqslant h\leqslant12$; $-12\leqslant k\leqslant12$; $-12\leqslant l\leqslant12$ |
| Reflections collected | 5693 |
| Independent reflections | 5532 ($R_{int}=0.94\%$) |
| Observed reflections | 5532 ($F\geqslant3.0\sigma(F)$) |
| Absorption correction | *N/A* |
| System used; solution | SHELXTL; direct methods |
| Refinement method | Full matrix, least squares |
| Quantity minimized | $\Sigma w(F_o-F_c)^2$ |
| Extinction correction | $\chi=-0.00021(12)$ where $F^*=F[1+0.002\chi F^2/\sin(2\theta)]^{-1/4}$ |
| Weighting scheme | $w^{-1}=\sigma^2(F)$ |
| Number of parameters refined | 106 |
| Final $R$ indices (observed data) | $R=5.32\%$, $wR=4.00\%$ |
| $R$ indices (all data) | $R=5.32\%$, $wR=4.00\%$ |
| Goodness of fit | 1.15 |
| Largest difference peak | 1.17 e $Å^{-3}$ |

TABLE 2

Positional parameters and thermal parameters $U_{ij}$[a] for $Ca_{8-x}Li_xAl_3$

| Atom | $x$ | $y$ | $z$ | SOF[b] | $U_{eq}$ | $U_{11}$ | $U_{22}$ | $U_{33}$ | $U_{23}$ | $U_{13}$ | $U_{12}$ |
|---|---|---|---|---|---|---|---|---|---|---|---|
| Ca1 | 0.47062(7) | 0.30106(7) | 0.35035(7) | 1 | 217(2) | 168(2) | 182(2) | 228(3) | 61(2) | 44(2) | 51(2) |
| Ca2 | −0.07839(7) | −0.22839(7) | 0.89231(7) | 1 | 194(2) | 193(2) | 225(3) | 222(3) | 101(2) | 93(2) | 134(2) |
| Ca3 | 0.12117(7) | −0.40216(7) | 0.35219(7) | 1 | 235(2) | 259(3) | 213(3) | 230(3) | 87(2) | 52(2) | 129(2) |
| Ca4 | 0.66387(7) | 0.12081(6) | 0.89032(7) | 1 | 211(2) | 187(2) | 167(2) | 245(3) | 70(2) | 37(2) | 81(2) |
| Ca5 | 0.04373(7) | 0.93931(7) | 0.33076(7) | 1 | 233(2) | 254(3) | 158(2) | 260(3) | 80(2) | 106(2) | 80(2) |
| Ca6 | 0.29947(6) | −0.50006(6) | 0.89163(7) | 1 | 208(2) | 144(2) | 183(2) | 250(3) | 40(2) | 80(2) | 57(2) |
| Ca7 | 0.22446(7) | −0.15364(9) | 0.69921(7) | 0.903(4) | 263(3) | 139(3) | 289(4) | 227(4) | −12(3) | 59(3) | 48(3) |
| Ca8 | 0.45202(9) | 0.28515(9) | 0.69999(8) | 0.938(4) | 270(4) | 373(4) | 375(4) | 241(4) | 156(3) | 147(3) | 292(3) |
| Al1 | 0 | 0.5 | 0 | 1 | 176(5) | 156(5) | 174(5) | 210(6) | 77(4) | 79(4) | 86(4) |
| Al2 | 0.5 | 0 | 0.5 | 1 | 195(5) | 222(5) | 155(5) | 207(6) | 60(4) | 99(5) | 90(4) |
| Al3 | 0.82818(9) | 0.66380(9) | 0.49990(10) | 1 | 176(3) | 130(3) | 149(3) | 214(4) | 66(3) | 32(3) | 54(3) |
| Al4 | 0.32348(9) | 0.15872(9) | −0.02741(9) | 1 | 177(3) | 158(3) | 159(3) | 206(4) | 62(3) | 73(3) | 73(3) |

[a]The $U_{ij}$ parameters are expressed in the form $\exp[-2\pi^2(U_{11}h^2a^{*2}+\ldots+2U_{12}hka^*b^*]$ and given in units of square picometres. Standard deviations are given in parentheses.

[b]Site Occupation Factor.

TABLE 3

Important bond distances (pm) in $Ca_{8-x}Li_xAl_3$

| Atom 1 | Atom 2 | Distance | Atom 1 | Atom 2 | Distance | Atom 1 | Atom 2 | Distance | Atom 1 | Atom 2 | Distance |
|---|---|---|---|---|---|---|---|---|---|---|---|
| Ca1 | Al2 | 353.3 | Ca4 | Al1 | 325.1 | Ca7 | Al2 | 342.3 | Al2 | Ca1 | 353.3 |
| | Al3 | 325.3 | | Al2 | 353.8 | | Al3 | 324.4 | | Ca1′ | 353.3 |
| | Al3′ | 354.4 | | Al4 | 363.3 | | Al4 | 325.4 | | Ca3 | 352.9 |
| | Al4 | 341.7 | | Al4′ | 321.8 | | Ca1′ | 386.1 | | Ca3′ | 352.9 |
| | Ca2′ | 365.3 | | Ca1′ | 376.9 | | Ca2 | 355.7 | | Ca4 | 353.8 |
| | Ca3′ | 390.8 | | Ca2′ | 360.9 | | Ca3 | 342.8 | | Ca4′ | 353.8 |
| | Ca4′ | 376.9 | | Ca3′ | 391.7 | | Ca3′ | 375.6 | | Ca5 | 402.2 |
| | a5 | 375.7 | | Ca5′ | 400.0 | | Ca4 | 351.6 | | Ca5′ | 402.2 |
| | Ca6′ | 362.2 | | Ca6′ | 372.0 | | Ca4′ | 381.6 | | Ca7 | 342.3 |
| | Ca7′ | 386.1 | | Ca7 | 351.6 | | Ca5 | 406.6 | | Ca7′ | 342.3 |
| | Ca8 | 343.4 | | Ca7′ | 381.6 | | Ca5′ | 397.8 | | Ca8 | 336.2 |
| | Ca8′ | 380.1 | | Ca8 | 353.7 | | Ca8 | 366.6 | | Ca8′ | 336.2 |
| Ca2 | Al1 | 330.2 | Ca5 | Al3 | 334.1 | Ca8 | Al2 | 336.3 | Al3 | Ca1 | 325.3 |
| | Al3 | 357.0 | | Al3′ | 337.1 | | Al3′ | 325.8 | | Ca1′ | 354.4 |
| | Al4 | 359.4 | | Al4′ | 367.8 | | Al4 | 326.5 | | Ca2 | 357.0 |
| | Al4′ | 315.4 | | Ca1 | 375.7 | | Ca1 | 343.4 | | Ca3 | 361.8 |
| | Ca1′ | 365.3 | | Ca2 | 399.2 | | Ca1′ | 380.1 | | Ca3′ | 326.2 |
| | Ca2′ | 390.6 | | Ca2′ | 370.4 | | Ca3′ | 378.7 | | Ca5 | 334.1 |
| | Ca3′ | 372.3 | | Ca3 | 372.2 | | Ca4 | 353.7 | | Ca5′ | 337.1 |
| | Ca4′ | 376.9 | | Ca4′ | 400.0 | | Ca5 | 411.8 | | Ca6′ | 356.1 |
| | Ca5 | 399.2 | | Ca5′ | 367.2 | | Ca5′ | 400.9 | | Ca7 | 324.4 |
| | Ca5′ | 370.4 | | Ca6′ | 372.7 | | Ca6 | 353.6 | | Ca8′ | 325.8 |
| | Ca6′ | 368.2 | | Ca7′ | 397.8 | | Ca6′ | 379.2 | | | |
| | Ca7 | 355.8 | | Ca8′ | 400.9 | | Ca7′ | 366.6 | | | |

(*continued*)

TABLE 3 (*continued*)

| Atom 1 | Atom 2 | Distance | Atom 1 | Atom 2 | Distance | Atom 1 | Atom 2 | Distance | Atom 1 | Atom 2 | Distance |
|---|---|---|---|---|---|---|---|---|---|---|---|
| Ca3 | Al1 | 318.8 | Ca6 | Al1 | 320.6 | Al1 | Ca2 | 330.2 | Al4 | CA1 | 341.7 |
| | Al2 | 352.9 | | Al3′ | 356.1 | | Ca2′ | 330.2 | | Ca2 | 359.4 |
| | Al3 | 361.8 | | Al4 | 358.8 | | Ca3 | 318.8 | | Ca2′ | 315.4 |
| | Al3′ | 326.2 | | Al4′ | 324.2 | | Ca3′ | 318.8 | | Ca4 | 363.3 |
| | CA1 | 390.8 | | Ca1′ | 362.2 | | Ca4 | 325.1 | | Ca4′ | 321.8 |
| | Ca2′ | 372.3 | | Ca2′ | 368.2 | | Ca4′ | 325.1 | | Ca5′ | 367.8 |
| | Ca4′ | 391.7 | | Ca3′ | 378.1 | | Ca6 | 320.6 | | Ca6 | 358.8 |
| | Ca5 | 372.2 | | Ca4′ | 372.4 | | Ca6′ | 320.6 | | Ca6′ | 324.3 |
| | Ca6′ | 378.1 | | Ca5′ | 372.7 | | | | | Ca7 | 325.4 |
| | Ca7 | 342.8 | | Ca6′ | 396.7 | | | | | Ca8 | 326.5 |
| | Ca7′ | 375.6 | | Ca8 | 353.6 | | | | | | |
| | Ca8′ | 378.7 | | Ca8′ | 379.2 | | | | | | |

Refinement of site occupation factors for the single crystal that was analysed revealed calcium deficiency. According to the data in Table 2, the resulting stoichiometry is $Ca_{7.84}Li_{0.16}Al_3$.

## 3. Analysis of the crystal structure

The structure of $Ca_{8-x}Li_xAl_3$, which is illustrated in Fig. 1, is quite complicated and seemingly unusual for an intermetallic compound. It adopts the triclinic space group, $P\bar{1}$, is isotypic to the reported structure of $Ca_8In_3$, and, as pointed out by Fornasini, is related to the f.c.c. $Fe_3Al$ structure type (also known as $Li_3Bi$ or $BiF_3$ type) [5]. It should be emphasized that we could only obtain this phase as a ternary compound. The close relationship between the $Ca_{8-x}Li_xAl_3$ structure and the $Li_3Bi$ type is clearly evident from the arrangement of aluminium atoms, which forms a slightly distorted f.c.c. framework where the coordination number of aluminium is 12 with distances 5.30 Å $\leqslant d$(Al–Al) $\leqslant$ 5.77 Å. The mean Al–Al distances for the four crystallographically different aluminium atoms differ by only 0.02 Å (5.51 Å $\leqslant d$(Al–Al) $\leqslant$ 5.53 Å).

The $Ca_8In_3$ and the $Ca_{8-x}Li_xAl_3$ structures are extraordinary examples of how to fill up an f.c.c. arrangement towards the composition $A_3B$. At first sight, the natural solution to this problem is the cubic $Li_3Bi$ structure where the lithium atoms completely occupy all tetrahedral and octahedral holes. However, there is certainly a very unfavourable situation for the lithium atoms in the octahedral sites because they are coordinated by eight atoms of the same type ($Li^{(T)}$) in the first sphere. Obviously, this can be overcome only in a few cases by the enormously favourable partial structure of the fluorite type, $A_2^{(T)}B$ or $Li_2^{(T)}Bi$. In some examples, extra stability is gained

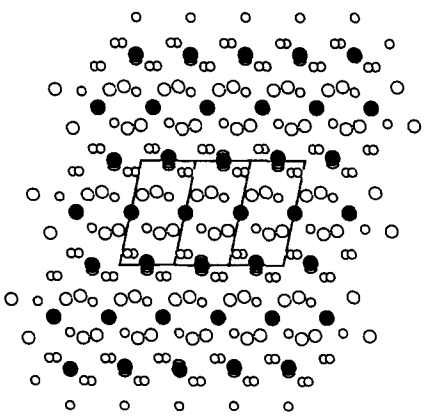

Fig. 1. The crystal structure of $Ca_{8-x}Li_xAl_3$ in a (010) projection: ●, aluminium atom positions; ○, Ca atoms originating from the tetrahedral holes of the $Li_3Bi$ structure type; ○, calcium or lithium sites originating from the octahedral holes in the $Li_3Bi$ type.

by introducing higher valent species at the tetrahedral positions as in $BiO_xF_{3-2x}$.

A competing solution is the $Na_3As$ structure with an h.c.p. array of arsenic atoms. Two-thirds of the sodium atoms occupy all tetrahedral holes, but the octahedral sites are vacant. The residual one-third of the sodium atoms are located halfway between the other sodium atoms to gain three near arsenic neighbours. The transition from the cubic $Li_3Bi$ type to the hexagonal $Na_3As$ type can be tuned experimentally in the series of phases $Li_{2x}Mg_{2-x}X$ (X≡Si, Ge) with increasing lithium content [6, 7]. Consequently, at the border between cubic and hexagonal structures, a regime of superstructures is observed. Driven by fulfilment of the octet rule and according to the Zintl–Klemm concept (for fundamental work, see ref. 8; about the 8-*N* rule see ref. 9), an increasing ratio of lithium with respect to magnesium in $Li^+_{2x}Mg^{2+}_{2-x}Si^{4-}$ results in an increasing population of the unfavourable octahedral sites.

Contrary to these silicides and germanides, the E13 compounds $Ca_8In_3$, $Ca_{8-x}Li_xAl_3$ and $Ca_{28}Ga_{11}$ belong to a class of intermetallic phases which do not obey strict valence rules. Applying the Zintl–Klemm concept, however, raises the question whether these compounds tend to follow the octet rule at all. The E13 elements, as they are the most electronegative species in the structures, have the role of the formal anions. They do not have homonuclear contacts E13–E13 and thus may be assumed to represent isolated $(E13)^{5-}$ octet systems. (The application of formal charges does not imply that these charges really exist. They are used to calculate the occupied orbitals which have their main contributions from the atomic orbitals of the most electronegative atoms. For semiconductors (Zintl phases) the orbitals are not different in number from the sum of orbitals of the free electronegative atoms [6, 8–11].)

The valence electron sums of the formal cations $Ca^{2+}$ and $Li^+$ and the formal charge acquisition sums of the E13 elements are collected in Table 4. It is interesting to note that the compound with gallium, which has the largest electronegativity in the series aluminium, gallium and indium, has the smallest number of excess electrons Δ needed to fulfil the octet rule. In other words, the gallium compound is closest to a Zintl phase or a semiconductor-like composition.

A comparison of the structures $M_8X_3$, $Li_3Bi$ and $Ca_{28}Ga_{11}$ is given in Fig. 2. The $M_8X_3$ structure is clearly related to the $Li_3Bi$ type, while the

TABLE 4

Application of the Zintl–Klemm concept to the $M_8X_3$ and the $Ca_{28}Ga_{11}$ structures

| Compound | Normal composition | $\Sigma q$(Ca, Li) | $q$(E13) | Δ |
|---|---|---|---|---|
| $Ca_8In_3$ | $Ca_{2.67}In$ | 5.33 | −5 | 0.33 |
| $Ca_{8-x}Li_xAl_3$ | $Ca_{2.61}Li_{0.05}Al$ | 5.27 | −5 | 0.27 |
| $Ca_{28}Ga_{11}$ | $Ca_{2.55}Ga$ | 5.10 | −5 | 0.10 |

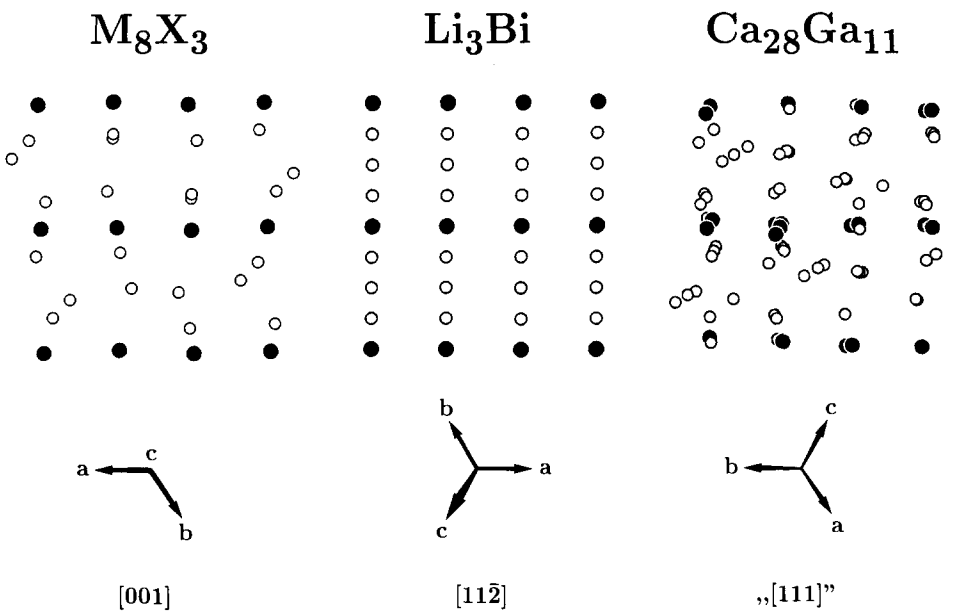


Fig. 2. Comparison of the structures of (a) $Ca_{8-x}Li_xAl_3$ ($M_8X_3$), (b) $Li_3Bi$ and (c) $Ca_{28}Ga_{11}$ in different projections to show the common building principle.

$Ca_{28}Ga_{11}$ arrangement is a fairly distorted variant, although the general formation of X layers (X≡In, Ga, Al, Bi) is obeyed in all three cases. Even the cation framework in $Ca_{8-x}Li_xAl_3$ (where calcium and lithium are represented by open circles) seems to be just slightly deformed from that of the cubic aristotype $Li_3Bi$ in this projection. The space near the unfavourable octahedral holes is no longer directly occupied, but the entire cationic network has rearranged in such a way that $2\frac{2}{3}$ cations per anion become acceptably coordinated by anions instead of just 2 in the case of $Li_3Bi$ (note: one-third of the cations in $Li_3Bi$ have eight close cation neighbours) (see Table 3). The coordination polyhedron of bismuth in the cubic structure is $Li_8$ cubes. One-sixth of the X atoms in $Ca_8In_3$ and $Ca_{8-x}Li_xAl_3$ still has this coordination (Al1). The environment of Al2 is an elongated icosahedron, while the other two aluminium sites have an irregular tenfold coordination with a cube-like appearance on one side and an icosahedral shape on the other. This figure is called the cubicosahedron [5]. These coordination polyhedra are shown in Fig. 3.

From inspection of Table 3, it becomes clear that the coordination of the calcium atoms by aluminium and other calcium atoms is different with either three or four close aluminium neighbours and eight or nine close calcium atoms. However, comparison of the individual atomic volumes by construction of Wirkungsbereiche (Dirichlet domains) [12–14] reveals strong similarities between the various calcium sites in this structure. (The volumes have been calculated by a FORTRAN 77 program [15] which uses a potential

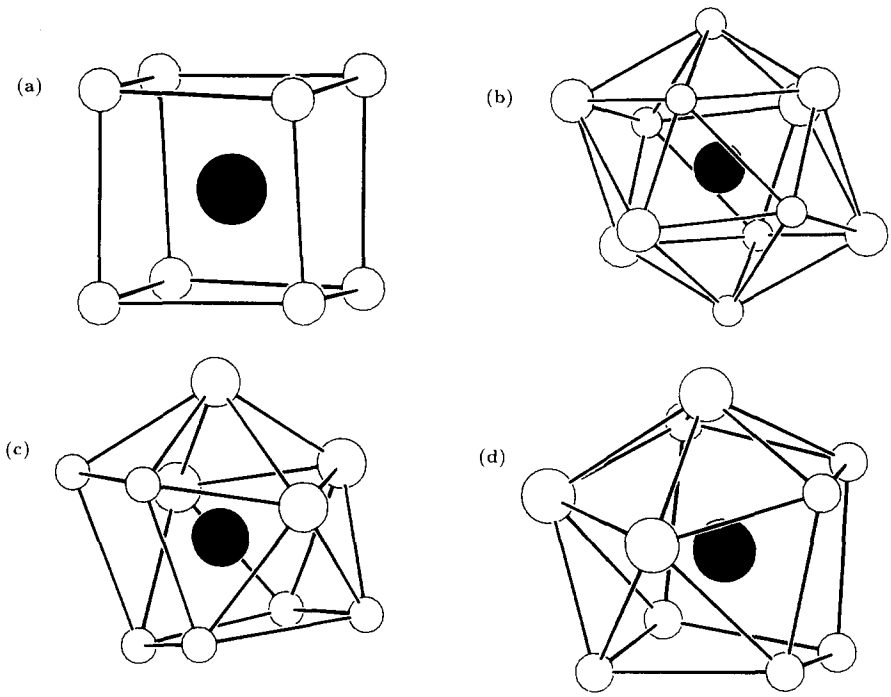


Fig. 3. The four different coordination polyhedra around each symmetry-inequivalent aluminium atom in $Ca_{8-x}Li_xAl_3$: (a) cube; (b) icosahedron; (c), (d) cubicosahedra.

plane construction for the generation of the domain boundary [14]. For the chosen atomic radii, a uniform value of $r = 1.0$ Å for all calcium and aluminium atoms was chosen.)

Although a common construction was applied for all atoms, calcium and aluminium atoms split into two separate volume regions. The differences for each of these is relatively small and varies between 33.1 and 35.7 Å$^3$ for calcium and between 29.0 and 31.1 Å$^3$ for aluminium (see Table 5). Similar results are also revealed by differences in other geometrical parameters, *e.g.* their mean effective "ionic" radii (MEFIR) and effective coordination numbers (ECON) [16], which are also tabulated in Table 5.

In addition to this geometrical analysis, local electrostatic potentials at the atomic sites in $Ca_{8-x}Li_xAl_3$ were evaluated using the Ewald method [17, 18] with formal charges of $-2.67$ and $+1.00$ assigned to aluminium and calcium or lithium respectively. The relative magnitudes of these site potentials $v$ (for cations $v<0$; for anions $v>0$) indicate the relative coordination of ions of one type (aluminium) by ions of the other type (calcium, lithium). Comparison of these results with the bond distances in Table 3 corroborates three close aluminium neighbours for Ca5, Ca7 and Ca8, and four close aluminium neighbours (all distorted tetrahedra) for Ca1, Ca2, Ca3, Ca4 and Ca6 sites. The crystal structure analysis indicated exclusive substitution by

TABLE 5

Site potentials $v$[a], partial atomic volume $V$, MEFIR [17] and ECON for $Ca_{8-x}Li_xAl_3$ ($x=0.16$)

| Atom | $v$[b] | $V$ (Å$^3$) | MEFIR | ECON | Coordination polyhedron |
|---|---|---|---|---|---|
| Ca1 | −0.500 | 33.4 | 1.79 | 11.3 | Irregular |
| Ca2 | −0.524 | 33.3 | 1.77 | 10.6 | Irregular |
| Ca3 | −0.532 | 33.2 | 1.77 | 10.6 | Irregular |
| Ca4 | −0.515 | 33.1 | 1.77 | 10.8 | Irregular |
| Ca5 | −0.483 | 35.7 | 1.86 | 13.0 | Irregular |
| Ca6 | −0.527 | 33.4 | 1.77 | 10.7 | Irregular |
| Ca7 | −0.489 | 33.2 | 1.75 | 10.1 | Irregular |
| Ca8 | −0.498 | 33.2 | 1.75 | 10.1 | Irregular |
| Al1 | 1.290 | 29.0 | 1.62 | 8.0 | Cube |
| Al2 | 1.256 | 31.1 | 1.75 | 10.8 | Pentagonal antiprism |
| Al3 | 1.272 | 29.5 | 1.68 | 9.37 | Cubicosahedron |
| Al4 | 1.281 | 29.4 | 1.67 | 8.90 | Cubicosahedron |

[a]From MAPLE calculations.
[b]Calculated with $q(Al) = -2.67$ and $q(Ca, Li) = +1.00$.

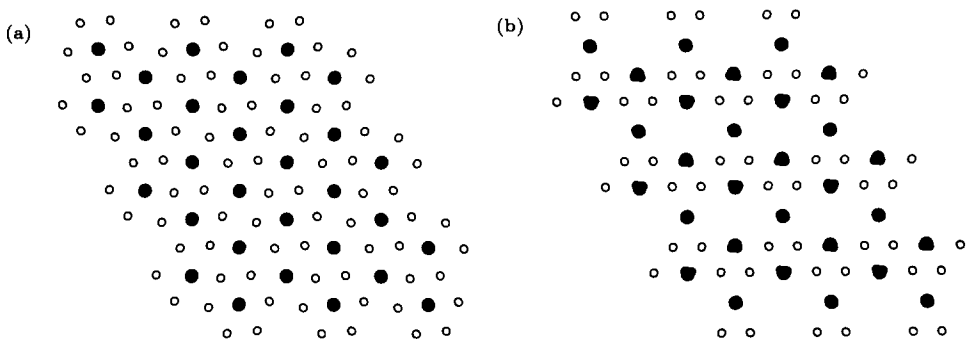


Fig. 4. (001) projections of the $Ca_{8-x}Li_xAl_3$ structure with only aluminium sites (●) and occupied $Ca^{(T)}$ sites (○) shown: (a) layer centred at $z=0$; (b) layer centred at $z=\frac{1}{2}$.

lithium at the Ca7 and Ca8 sites, which we would expect on the basis of their smaller site potential values, although Ca5 sites show no lithium substitution. Plots of aluminium polyhedra around the Ca5, Ca7 and Ca8 sites at distances out to 600 pm reveal that these three positions have shifted away from the centres of aluminium octahedra. Therefore we can formulate $Ca_{8-x}Li_xAl_3$ as $(Ca,Li)_3{}^{(O)}(Ca)_5{}^{(T)}Al_3$ with respect to the $Li_3Bi$ structure type, and recognize that lithium substitutes at the octahedral sites and the vacancies occur at the tetrahedral sites.

The arrangement of vacancies is readily observed by considering the two layers of Al atoms centred at $z=0$ and $z=\frac{1}{2}$ and their $Ca^{(T)}$ neighbours. Figure 4 illustrates these two sheets in a (001) projection, which show pairs of vacancies in the $z=\frac{1}{2}$ layer. This configuration of vacancies results in all

aluminium atoms in this sheet being six coordinate to $Ca^{(T)}$ rather than eight coordinate (as in $Li_3Bi$): one-third of the aluminium atoms with vacancies diagonally opposite (Al2) and two-thirds of the aluminium atoms with vacancies on an edge of the cube (Al3). This arrangement of defects also effects coordination vacancies for aluminium atoms in the $z=0$ layer: one-third of them remaining eight-coordinate cubic, but two-thirds having a single vacancy–seven coordinate by $Ca^{(T)}$. Madelung calculations on different defect arrangements in the $Li_3Bi$-type framework indicated that the observed vacancy ordering in $Ca_{8-x}Li_xAl_3$ is one of the least favoured configurations — the most favourable energies occurred for those patterns in which the vacancies were isolated from each other as far as possible, although the calculated energy differences were no larger than about 1.5 eV. Upon distortion to the actual geometry of these $M_8X_3$ compounds, the Madelung term dropped by several electronvolts. Structurally, the $M^{(O)}$ sites contract around the vacancy pairs, which results in a more uniformly distributed cationic coordination environment around each X centre (see Table 5).

## 4. Extended Hückel investigations

Electronic structure calculations using the extended Hückel ansatz [19] were carried out on an $Li_3Bi$-type "$Ca_3Al$", a defect "$Ca_3Al$", $Ca_{3-x}Al \equiv Ca_8Al_3$, and the actual $Ca_8Al_3$ structure in order to examine the deviations from the Zintl–Klemm ideas presented in Table 4. That is, what is the nature of the additional electrons beyond the formal octet at the E13 element? These calculations utilized the tight-binding method with a special points set of $k$ points in the irreducible wedge of the first Brillouin zone (between 150 and 400 points). The structural parameters from $Ca_{7.84}Li_{0.16}Al_3$ were used for $Ca_8Al_3$, and cell parameters for the other two structures were determined to maintain equal cell volumes per number of aluminium atoms. Atomic parameters are listed in Table 6.

Figure 5 shows the density of states (DOS) curves for the three structures and highlights the contribution from the $Ca^{(O)}$ orbitals to the total DOS. Clearly, the distribution of defects does not enhance the electronic stability of a fictitious "$Ca_3Al$", but the final relaxation of the $Ca^{(O)}$ atoms around

TABLE 6

Atomic parameters used in the extended Hückel calculations

| Atom | Orbital | Energy (eV) | Exponent $\zeta$ |
|---|---|---|---|
| Al | 3s | −12.30 | 1.37 |
| | 3p | −6.50 | 1.36 |
| Ca | 4s | −7.00 | 1.10 |
| | 4p | −4.00 | 1.10 |

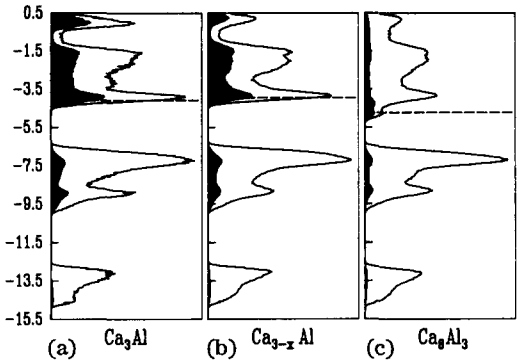


Fig. 5. Total DOS for "$Ca_3Al$" in (a) the $Li_3Bi$ structure, (b) the "$Ca_{3-x}Al$" structure undistorted, and (c) $Ca_8Al_3$ in the observed $Ca_{7.84}Li_{0.16}Al_3$ structure: ■, projected DOS from the $Ca^{(O)}$ sites; – – –, respective Fermi levels determined for 8.33 electrons per aluminium atom. Energies are in units of electronvolts.

the vacancies produces significant stability – the calculated Fermi levels (noted by the broken lines for 8.33 electrons per aluminium atom) differ by nearly 0.75 eV. Evaluation of overlap populations between various sets of Ca–Al and Ca–Ca pairs indicates that the occupied part of the conduction band in the $Ca_8Al_3$ structure is Ca–Al nonbonding and Ca–Ca bonding. As the figure shows, most of the DOS in this energy region is centred on the $Ca^{(O)}$ atoms. Although there are no definitive clusters of calcium and lithium in $Ca_{8-x}Li_xAl_3$, this result is consistent with earlier investigations on the lithium-rich silicides $Li_{21}Si_5$ [20] and $Li_{12}Si_7$ [21].

Furthermore, a Mulliken population analysis supports the conclusions from the Madelung calculations. In "$Ca_3Al$", the total charges on the two different metal sites were 1.25 and 1.02 for $Ca^{(T)}$ and $Ca^{(O)}$ respectively, whereas in $Ca_8Al_3$, the corresponding populations varied between 1.24 and 1.28 for $Ca^{(T)}$ and between 1.17 and 1.30 for $Ca^{(O)}$.

## 5. Conclusions

The structure of $Ca_{8-x}Li_xAl_3$ ($x = 0.16$) was determined to be isostructural with an analogous binary compound $Ca_8In_3$, although no corresponding binary Ca–Al phase could be isolated. The structure is a defect variation of the cubic $Li_3Bi$ structure type with lithium substituting for calcium at the octahedral sites (4b in $Fm\bar{3}m$) and vacancies occurring in the tetrahedral sites (8c in $Fm\bar{3}m$). Due to the lower site potentials at the 4b sites, we rationalize the lithium substitution, but the defect pattern arises for structural and electronic reasons. The relaxation of the 4b atoms around the vacancies effects a uniform charge distribution surrounding each aluminium atom as well as stabilizing the bottom of the conduction band by introducing occupied Ca–Ca bonding orbitals.

This class of compounds comes close to following the Zintl–Klemm concepts with the additional electrons involved in cation–cation bonding states. Reports of $LiMg_2Ga$ and $Li_2MgGe$ which adopt the $Li_3Bi$ structure with an ordering of cations [22] are also consistent with our observation that the gallides come closest to fulfilling the octet rule, in accordance with electronegativity trends of the group 13 elements.

## Acknowledgments

We thank Professor H. G. von Schnering for his continued support and enthusiasm, and Jan Curda for synthesis and initial identification of this phase.

## References

1 R. Nesper and G. J. Miller, in preparation.
P. Villars and L. D. Calvert, *Pearson's Handbook of Crystallograpic Data for Intermetallic Phases*, Vol. 2, American Society for Metals, Metals Park, OH, 1989, p. 914, and references cited therein.
2 J. B. Friauf, *J. Am. Chem. Soc.*, *49* (1927) 3107.
3 H. Nowotny, E. Wormnes and A. Mornhein, *Z. Metallkde.*, *32* (1940) 39.
4 M. L. Fornasini and M. Pani, *Acta Crystallogr. C*, *42* (1986) 394.
5 M. L. Fornasini, *Acta Crytallogr. C*, *43* (1987) 613.
6 R. Nesper, *Habilitationschrift*, Universität Stuttgart, 1988.
7 R. Nesper and J. Curda, *Diskussionstagung der Arbeitsgemeinschaft Kristallographie*, Konstanz, 1988, p. 196; *Z. Kristallogr.*, *182* (1988) 196.
8 E. Zintl and G. Brauer, *Z. Phys. Chem., Abt. B*, *20* (1933) 245.
E. Zintl, *Angew. Chem.*, *52* (1939) 1.
W. Klemm, FIAT-review of German science, Naturforschung und Medizin in Deutschland 1939–1946, *Anorg. Chem., Teil IV*, *26* (1949) 103.
9 W. Klemm, *Trab. Reun. Int. React. Sólidos*, *1* (1956) 447; *Proc. Chem. Soc. London*, (1956) 329; *Festkörperprobleme Vieweg*, Braunschweig, 1963.
E. Mooser and W. B. Pearson, *Phys. Rev.*, *101* (1956) 1608; *Prog. Semicond.*, (1960) 103.
E. Busmann, *Z. Anorg. Allg. Chem.*, *313* (1961) 90.
10 R. Nesper, *Prog. Solid State Chem.*, *20* (1990) 1.
11 R. Nesper, *Angew. Chem.*, *103* (1991) 805; *Angew. Chem. Int. Edn. Engl.*, *30* (1991) 789.
12 P. Niggli, *Z. Kristallogr.*, *68* (1928) 404.
13 F. Laves, *Z. Kristallogr.*, *78* (1931) 208.
14 W. Fischer, E. Koch and E. Hellner, *Neues Jahrb. Mineral., Monatsh.*, (1971) 227.
15 K. Wohlfart, B. Neukäter and H. G. von Schnering, *Programme zur Berechnung konvexer Polyeder*, Universität Münster, Münster, 1967.
R. Nesper and U. Häussermann, *Verbesserte Programmversion*, Eidgenössirche Technische Hochschule, Zürich, 1991.
16 R. Hoppe, *Angew. Chem.*, *82* (1970) 7; *Angew. Chem. Int. Edn. Engl.*, *9* (1970) 25; *Z. Kristallogr.*, *150* (1979) 23.
17 P. P. Ewald, *Ann. Phys.*, *64* (1921) 253.
18 R. Hoppe, *Angew. Chem.*, *78* (1966) 52; in O. C. J. M. Rooymans and A. Rabenau (eds.), *Crystal Structure and Chemical Bonding in Inorganic Chemistry*, North-Holland, Amsterdam, 1975.

G. Roch, W. Neukäter and H. G. von Schnering, *Programm zur Berechnung von Gitterpotentialen und Madelungfaktoren*, Universität Münster, Münster, 1962.
R. Nesper, *Modifizierungen zur Berechnung von Potentialdichten*, Max-Planck-Institut für Festkörperforschung, Stuttgart, 1984.
R. Nesper and H. Meyer, *Verbesserte Programmversion*, Eidgenössirche Technische Hochschule, Zürich, 1991.
19 R. Hoffmann, *J. Chem. Phys.*, *39* (1963) 1397.
J. Ammeter, H.-B. Bürgi, J. C. Thibeault and R. Hoffmann, *J. Am. Chem. Soc.*, *100* (1978) 3686.
20 R. Nesper and H. G. von Schnering, *J. Solid State Chem.*, *70* (1987) 48.
21 R. Nesper, H. G. von Schnering and J. Curda, *Chem. Ber.*, *119* (1986) 3576.
22 H. Pauly, A. Weiss and H. Witte, *Z. Metallkde.*, *59* (1968) 414.